Geoderma 467 (2026) 117738

Contents lists available at ScienceDirect

Geoderma

journal homepage: www.elsevier.com/locate/geoderma

Multispectral bare soil composites as a resource for SOC mapping rather than SOC monitoring: A case study in the Walloon region (Belgium)

Dries De Bièvre *, Pierre Defourny, Bas van Wesemael

Earth and Life Institute, Université Catholique de Louvain, Louvain-la-Neuve, 1348, Belgium

ARTICLE INFO

Handling Editor: Brandon Heung

Keywords:
Soil organic carbon
Optical remote sensing
Geostatistics
Machine-learning
Soil health

ABSTRACT

Soil organic carbon (SOC) is a key indicator of soil health on croplands, as well as a potential lever for carbon sequestration in agriculture. This requires tools for understanding spatial and temporal variations in SOC content. Multispectral satellites provide data on bare soil reflectance which is influenced by SOC content. In this study, an extensive database of 34,418 soil analyses on 22,850 fields is leveraged to train a Machine-Learning model for SOC content prediction. The predictive covariates are derived from a bare soil composite of Sentinel-2 images over the Walloon region (Belgium) obtained from March to June over a three-year period (2019–2021) as well as some environmental covariates. We observe that multispectral data is complementary to environmental covariates for explaining spatial variability in SOC content. Through feature elimination relevant spectral features were identified: the normalized difference of band 3 (Green) and 2 (Blue); band 5 (Red-Edge) and 11 (SWIR1); band 11 (SWIR1) and 12 (SWIR2) and the reflectance in band 4 (Red). These spectral indices were combined with three environmental covariates: elevation, the agro-ecological zone and the fine fraction (< 20μm) content. The resulting model predicts SOC content at field-level with an RMSE of 2.7 g C kg^{-1} and an R^2 of 0.56. Given this uncertainty, we conclude that multispectral data is insufficient for SOC content monitoring at parcel-level but is a tool to consider for SOC content mapping. The SOC content map can be used for regional SOC content estimates, after modeling the autocorrelation of the model errors. This offers the possibility to compare groups with different management practices or assess the average SOC content of fields in a soil conservation program compared to a regional baseline.

1. Introduction

The soil is a valuable natural resource that plays a central role in ecosystem functioning, as the place where atmosphere, biosphere and hydrosphere interact. Soil organic matter (SOM) plays a key role in this respect, influencing infiltration capacity, water retention, soil structure, nutrient availability, and soil aeration.

Conversion of natural vegetation to croplands typically causes a reduction in organic matter (Guo and Gifford, 2002). Soils under intensive agriculture are at risk of further losing organic matter, causing land degradation. Therefore, policymakers are interested in incentivizing land users to increase Soil Organic Carbon (SOC) levels with dedicated agricultural practices. Specifically in the European Union, this is reflected in the proposed 'Soil Monitoring Law' (European Commission, 2023). On the other hand, in the context of climate change mitigation, agricultural soils are identified as a potential carbon sink (Lal, 2018). Initiatives to reward farmers for carbon sequestration in the voluntary carbon market are being set up, referred to as 'carbon farming' (Johansson et al., 2024). This requires developing the capacity to accurately monitor carbon dynamics in croplands, in space and time, and at a spatial resolution equal to or smaller than agricultural parcels to differentiate between fields with different management practices. Besides, knowledge on the natural variation of SOC content in croplands is relevant to define regional baselines which allow to evaluate the effectiveness of agricultural practices for increasing SOC content (Lugato et al., 2014; Viscarra Rossel et al., 2014).

The current standard for mapping soil properties is using the relation between soil-forming factors and the soil property. This approach is referred to as digital soil mapping (DSM) (McBratney et al., 2003). In the Walloon Region (Belgium), DSM allowed to map the SOC stocks in croplands and grasslands at a spatial resolution of 40 m with an R^2 of 0.64 (Chartin et al., 2017). However, agricultural practices which impact the carbon balance are often not reflected in these models. These management decisions are made at the parcel level and can induce changes in SOC between fields in the same environmental conditions. Models that include management variables allow for higher precision when mapping SOC content (Zhou et al., 2022). Data on

* Corresponding author.
E-mail address: dries.debievre@uclouvain.be (D.D. Bièvre).

https://doi.org/10.1016/j.geoderma.2026.117738
Received 15 October 2025; Received in revised form 8 January 2026; Accepted 11 February 2026
Available online 27 February 2026

these management practices are not readily available and not standardized over larger areas. This is an information gap that could be addressed through the use of earth observation to obtain harmonized information on crop rotation, presence of cover crops and residues for example d'Andrimont et al. (2021), Fendrich et al. (2023) and Hively et al. (2018).

As an alternative to mapping SOC content through its correlation with soil-forming factors, SOC content may directly be estimated from the reflectance signal of bare soil, following the principles of soil spectroscopy. Soil spectroscopy has emerged as a more affordable, non-destructive alternative to chemical soil analysis. Soil properties can be estimated from the reflectance signature of the soil due to the relation between soil components and the reflectance in the visible (Vis), Near-Infrared (NIR) and Short-Wave-Infrared (SWIR) range of the electro-magnetic spectrum. This has been well established for spectra measured in laboratory conditions, using hyperspectral measurements on dried and crushed samples (Stenberg et al., 2010). Organic material is known to decrease the albedo of the soil and specifically affect absorption in the SWIR range of the spectrum. This allows to estimate SOC content using Vis-NIR spectroscopy (Nocita et al., 2013; Stevens et al., 2013, 2008). Soil spectroscopy builds on spectral libraries to train predictive models. At the European scale, a local Partial Least Squares Regression (PLSR) model allowed to estimate carbon content on croplands with an RMSE of 3.6 g C kg^{-1} and an R^2 of 0.84 (Nocita et al., 2014). A PLSR model trained on a Walloon database predicts SOC contents with an RMSE of 3.2 g C kg^{-1} (Castaldi et al., 2018).

Since satellites with optical sensors measure reflectance with wide coverage and high spatial and temporal resolution, this creates an opportunity for estimating soil properties over large areas. Under the European Copernicus program, the Sentinel-2 mission provides data that can be exploited for SOC content mapping. Previous research has led to methods for extracting bare soil pixels with minimized disturbance from high soil moisture and crop residues by filtering on spectral indices (Demattê et al., 2018; Dvorakova et al., 2021; Rogge et al., 2018). To increase the coverage of the map, multiple observation dates are combined into a multitemporal bare soil composite (Castaldi et al., 2019; Dvorakova et al., 2020, 2021, 2023; Shi et al., 2022; Zepp et al., 2021). Different approaches have been developed which differ in the spectral indices used for masking and their thresholds (Demattê et al., 2018; Heiden et al., 2022; Rogge et al., 2018). Vegetation is masked using a threshold on the Normalized Difference Vegetation Index (NDVI). Yet soil moisture content, crop residues, surface roughness and soil crusts all impact the reflectance spectrum and different filters to mask affected pixels can be used. Dvorakova et al. (2021) show that selecting soils in seedbed conditions strongly improves the model but reduces data availability. Methods for obtaining a bare soil composite should also be adapted to the study area, since the soil type affects the optimal threshold values (Broeg et al., 2024; Heiden et al., 2022). Correcting for potential soil moisture effects by including Sentinel-1 derived soil moisture products as covariates did not allow to improve model performance in France (Urbina-Salazar et al., 2021).

Statistical models then need to be trained on the reflectance values of the bare soil composite. PLSR, being a popular method in soil spectroscopy, has also been applied to multispectral data (Dvorakova et al., 2021). It assumes linear relationships and is designed for data with many correlated features. PLSR is thus rather suited for hyperspectral data than for multispectral data. Machine learning techniques, such as random forests have also been applied (Breiman, 2001; Heil et al., 2022; Urbina-Salazar et al., 2023; Zepp et al., 2021). These are powerful tools to model complex relationships and also allow to make model-free estimates of uncertainty with the use of quantile regression approaches (Meinshausen and Ridgeway, 2006; Urbina-Salazar et al., 2023; Vaysse and Lagacherie, 2017). These flexible machine learning algorithms, however, require larger amounts of training data compared to PLSR and are less straightforward to interpret. Other approaches used for soil property prediction include cubist regression, support vector machines and neural networks (Biney et al., 2021; Mzid et al., 2022; Samarinas et al., 2023; Tziolas et al., 2024; Žížala et al., 2019).

A recurring challenge for calibrating models for SOC prediction is the skewed distribution of SOC contents in croplands making high SOC values lacking in the training data. As a consequence, high SOC values tend to be underestimated by models, also indicating that the signal-to-noise ratio is small (Broeg et al., 2024; Samarinas et al., 2023; Urbina-Salazar et al., 2023). Therefore, the study area can strongly influence model performance. SOC mapping works best in areas where there is enough SOC variability, yet low variability in confounding factors (Chabrillat et al., 2019; Vaudour et al., 2022). Usually, single models over large areas perform poorly and local regression techniques or ensemble models allow to adapt to different local conditions in the study area (Broeg et al., 2024; Nocita et al., 2014; Stevens et al., 2013; Viscarra Rossel et al., 2024). For example at the European scale, a model on Landsat imagery only achieves an R^2 of 0.06 (RMSE = 16.8 g C kg^{-1}), the more recent WorldSoils map based on Sentinel-2 imagery reports an R^2 of 0.41 (yet with RMSE = 18.07 g C kg^{-1}) (Safanelli et al., 2020; van Wesemael et al., 2024).

Interpretation of the prediction models has been lacking in previous studies (Broeg et al., 2024; Dvorakova et al., 2023; Urbina-Salazar et al., 2023; van Wesemael et al., 2024). Most models using Sentinel-2 data either use only the 10 reflectance bands as predictors or a larger set of spectral indices in a 'black-box' model. Feature selection algorithms can be used to select a limited number of predictive features among many possible spectral indices, thereby facilitating interpretation, however requiring a large amount of data. When combining this with techniques for the interpretation of machine-learning models, an in-depth interpretation of the SOC prediction model can be done (Wadoux et al., 2023; Wadoux and Molnar, 2022). Understanding the model helps to avoid overfitting or the inclusion of covariates without a physical relation with SOC content (Wadoux et al., 2020).

SOC content maps can have applications at different spatial supports and be used either for monitoring, when explaining temporal variability, or for mapping, when explaining spatial variability. Bare soil composites are sometimes presented as a tool for parcel-level, SOC content monitoring. However, it is not clear whether the accuracy is sufficient. There is a trade-off between the spatial resolution and precision, where spatial aggregation reduces the variance of the SOC content estimate (Padarian and McBratney, 2023). Spatial averages can also be useful to reduce sampling needs for regional SOC content monitoring or to set regional SOC content baselines (Wadoux et al., 2024). The value of multispectral bare soil composites for regional applications is however still unclear.

In this study, three objectives are addressed over a heterogeneous study area of 16 000 km^2, i.e. the Walloon Region (Southern part of Belgium):

i. Identify spectral features that are important for SOC content prediction and understand the physical explanation for their importance.
ii. Assess the value of a bare soil composite for SOC content mapping and/or monitoring in the Walloon region at parcel-level.
iii. Assess the precision of spatial averages derived from parcel-level predictions.

2. Materials and methods

2.1. Study area

The Walloon region in southern Belgium covers about 16,900 km^2, nearly half of which is devoted to agriculture. The physical environment changes noticeably from north to south: in the lowland areas north of the Sambre and Meuse rivers, sandy loam and silty soils support intensive crop production, while the southern uplands are cooler and wetter, with shallow, stony soils that favor grassland, forests,

Table 1
Spectral bands of the Multispectral Imager aboard the Sentinel-2 satellites.
Source: sentiwiki.copernicus.eu.

Band number	Spectral range[a] (nm)	Spatial resolution (m)
2–Blue	460–525	10
3–Green	543–578	10
4–Red	650–680	10
5–Red-Edge	697–711	20
6–Red-Edge	733–748	20
7–Red-Edge	773–792	20
8A–Red-Edge	854–875	20
8–Near-Infrared	780–885	10
11–Short-Wave Infrared 1	1568–1659	20
12–Short-Wave Infrared 2	2110–2290	20

[a] Spectral ranges are approximate.

and extensive cattle raising. Soil types also vary across the region, ranging from Haplic Luvisols in the north to Distric Cambisols in the south, with Fluvisols along the valley bottoms (Chartin et al., 2017). Based on these natural and agronomic conditions, Wallonia is divided into ten agricultural regions, reflecting the gradient of soils, climate, and land use across the landscape (Goidts and van Wesemael, 2007).

2.2. Sentinel-2 bare soil composite

Bare soil composites were generated from multispectral Sentinel-2 images for a period of three years (2019, 2020, 2021), using the Google Earth Engine platform. Images acquired between March 1st up to June 30th, with a cloud coverage smaller than 50%, were selected. This reduces errors from atmospheric correction, which are more prevalent in cloudy images, and excludes winter images which tend to have higher soil moisture, higher solar zenith angle and higher soil roughness (Vaudour et al., 2019). Pixels with a cloud probability larger than 10%, assessed by the s2cloudless algorithm, were masked (Skakun et al., 2022). Cloud shadows were masked by applying a filter to pixels with reflectance below 0.15 in Band 8 (NIR), located within 1 km of a cloud pixel and positioned opposite to the mean solar azimuth angle (Google Earth Engine Developers, 2025).

On the resulting images, pixels with an NDVI smaller than 0.25 and an NBR2 smaller than 0.05 were identified as bare soil. These thresholds are based on field observations in the Walloon region (Dvorakova et al., 2023). The bare soil multispectral composite was then calculated as the median bare soil reflectance value for each band, in each pixel. Pixels in the composite that were calculated based on a single image were also masked in the final composite. Bands 2, 3, 4, 5, 6, 7, 8, 8A, 11 and 12 were retained in the bare soil composite (Table 1).

Since SOC data was available at field level, the bare soil reflectance was aggregated by field using the Land Parcel Information System (LPIS) of 2020. A buffer of 20 m around the field borders was applied to reduce edge effects. If more than 80% of the remaining surface was covered by the bare soil composite, the composite pixels inside the field were averaged to obtain the average bare soil reflectance of that field, for each of the 10 spectral bands.

2.3. Soil data

SOC content data from a database of routine soil analyses were used to train and validate SOC prediction models. The dataset was provided by the Belgian REQUASUD network of soil laboratories, providing soil fertility analyses to farmers. A dataset of 34,418 geolocated samples was available over the period 2018–2021 on croplands. The soil map of Belgium was used by REQUASUD to assess the homogeneity of a parcel. In homogeneous fields, 1 composite sample was acquired, while in heterogeneous fields different samples were acquired, each representing a homogeneous zone. At the time of sampling, GPS coordinates were recorded in the area where the sample was collected. Representative samples of the parcel were obtained through systematic sampling of 5 points in an approximate W-shape covering the parcel and mixing these to a composite sample. Sampling was done to a depth of 25 cm. SOC content was analyzed using either the Springer Klee method or the dry combustion method. The dataset has been described by Zhou et al. (2022).

The coordinates of the samples analyzed between 2018 and 2021 were compared to the field delineations the LPIS of 2020. Within this 4-year period no large changes in SOC content are expected. Comparing the location of the samples to the LPIS, resulted in 22,850 fields with at least one SOC measurement. Fields with multiple measurements and a SOC range larger than 5 g C kg^{-1} were removed. These differences may be due to within field heterogeneity. For the other fields the SOC content was estimated by the average of the available samples, if there was more than 1 sample available. Fields smaller than 1 ha were excluded because boundary effects strongly affect the soil reflectance for small fields. This resulted in a dataset of 16,258 fields with a SOC estimate (Fig. 1). From 16,258 fields with measured SOC content, 14,173 fields were represented in the bare soil composite. The other fields have either not been bare in the period 2019 to 2021 or cloud coverage hindered their observation. The 14,173 fields were partitioned into a calibration set and a validation set using a random 80/20 split, producing 11,318 fields for calibration and model comparison (calibration set) and 2855 fields for validation (validation set) (Fig. 1).

2.4. Geospatial covariates

Four geospatial covariates were used additionally to the spectral predictors: agro-ecological zones, the fine fraction content (<20 μm), elevation and the topographic wetness index. These four variables are expected to reflect variability in soil type, dominant cropping system, soil texture, average temperature, precipitation and local topography. With these covariates the scorpan factors are covered while avoiding model complexity and risk of overfitting (McBratney et al., 2003). Elevation is correlated to climatic variables (temperature and precipitation) in this area and thus for simplicity temperature and precipitation were not included (Chartin et al., 2017). AEZs were used to encode for both soil type and differences in agricultural practices and thus anthropogenic factors. With this selection of covariates a balance in the complexity between the two approaches (DSM and spectral) is pursued. Despite the high number of spectral features, they are strongly correlated. There would then be a risk in comparing this approach to a DSM model with a large set of less correlated covariates which may perform well due to overfitting. The source and processing of each covariate is explained in the following sections.

2.4.1. Agro-ecological zones (AEZs)

The AEZs were derived from the official ten agricultural regions of the Walloon region (wallex.wallonie.be). Since some areas have a low occurrence of croplands, the original agricultural regions were regrouped, combining regions according to similarity in soil types, to ensure sufficient samples in each zone. The resulting AEZs are shown in Fig. 2.

2.4.2. Estimated content of the fine soil fraction (<20 μm)

A map of the fine soil fraction is available on the data portal of the Walloon region (geoportail.wallonie.be) at a spatial resolution of 50 m. This data was obtained using regression kriging of 6129 historical soil profiles from the Belgian AardeWerk database (Chartin et al., 2017). The layer has been a significant predictor for mapping SOC stocks in a DSM model (Chartin et al., 2017). For each parcel the average content was derived as the average pixel value inside the polygon.

2.4.3. Elevation

The average elevation of the parcels in the LPIS 2020 was derived from the FABDEM global digital elevation model (Hawker et al., 2022).

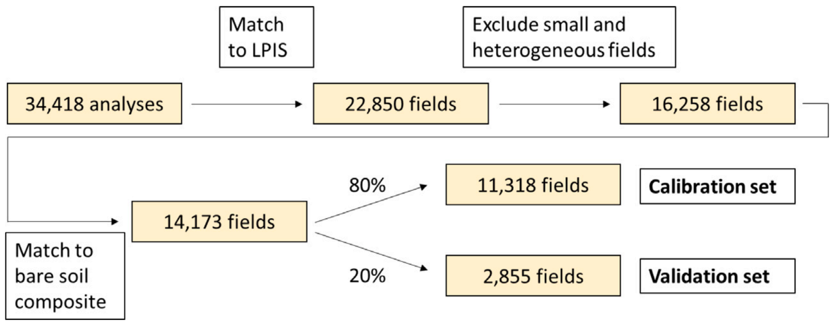

Fig. 1. Schematic representation of the data cleaning and splitting, combining spectral data and soil analyses for calibration and validation of Soil Organic Carbon content prediction models. Acronyms: LPIS, Land Parcel Information System.

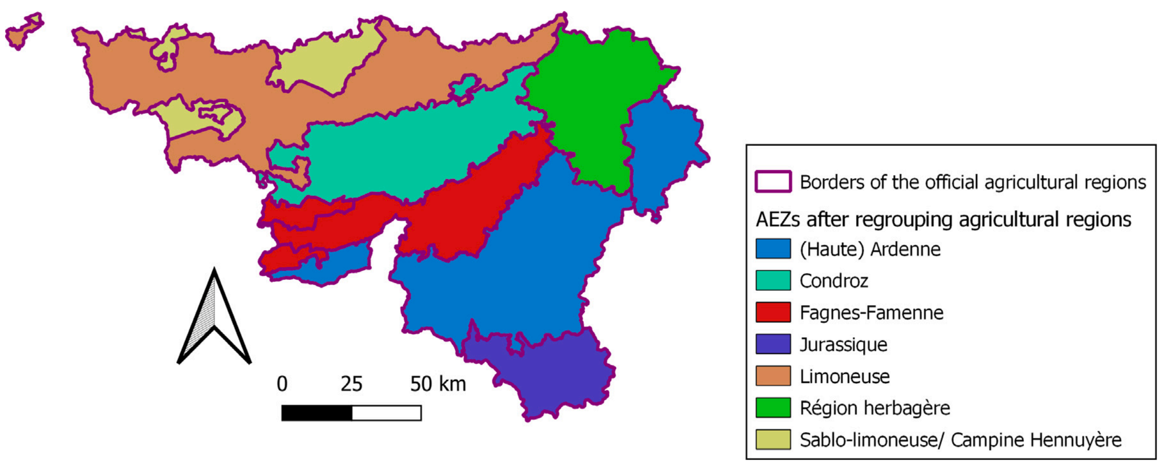

Fig. 2. Agro-ecological zones (AEZs) obtained by regrouping the agricultural regions of Belgium for the Walloon region.

2.4.4. *Topographic Wetness Index (TWI)*

The TWI was calculated according to Eq. (1), where a is the local upslope contributing area and b the local slope in radians (Beven and Kirby, 1979). Consequently, the TWI was averaged per parcel.

$$TWI = \ln \frac{a}{\tan b} \tag{1}$$

2.5. *Model comparison*

Prediction models were estimated using the Random Forest (RF) regression model accessible in the scikit-learn package for Python (Pedregosa et al., 2011). RF regression models consist of an ensemble of regression trees, making the model more robust to overfitting (Breiman, 2001).

To assess the value of Sentinel-2 bare soil spectra for mapping SOC contents, models based on three distinct sets of predictors were compared. The first set (SPEC) consists of the variables derived from the bare soil composite. This includes the reflectance in each of the 10 bands mentioned in Table 1. Additionally, 90 spectral indices were considered. These indices were the average reflectance (Eq. (2)) and normalized difference (Eq. (3)) of all pairwise combinations of the 10 spectral bands. On the resulting set of 100 predictors, recursive feature elimination (RFE) was performed in each fold of cross-validation to select ten features for fitting the model. RFE is an iterative process where at each step, the features with smallest feature importance are removed starting from the full model. To save computational resources, the RFE algorithm was implemented to remove the 20 least informative features per step until selecting 20 features. From these 20 features, RFE was applied to remove one feature per step until ten features were selected. An exploratory analysis proved that the reduction in R^2 from the full model to a model with ten features was not significant.

$$Pairwise\ average\ (avg) = \frac{\rho_i + \rho_j}{2} \tag{2}$$

$$Normalized\ difference\ (ND) = \frac{\rho_i - \rho_j}{\rho_i + \rho_j} \tag{3}$$

The second set of predictors (GEO) consisted of the four geospatial covariates: the average elevation of the field, the average TWI, the AEZ and the average fine fraction (<20 μm) content. The AEZ was encoded using simple target encoding (Pargent et al., 2022). The third set of predictors (SPEC+GEO) was obtained by combining the spectral variables and environmental covariates, resulting in 104 features. Therefore, the same RFE protocol was applied to select ten features. For the SPEC and SPEC+GEO models, RFE was included in the cross-validation procedure. The number of folds in which a feature was selected, was then used to select a limited set of important features for a more parsimonious model. This model was then evaluated on the validation set of 2855 observations and used for mapping, and will therefor be referred to as MODEL_MAP.

The models were evaluated by five-fold cross-validation on the training set. For each fold, the R^2 and Root Mean Square Error (RMSE) were calculated on the held-out data, on the observed SOC content (SOC_o), predicted SOC content (SOC_p) and the number of observations in the subset (N) (Eqs. (4) and (5)). For each fold, the R^2 and RMSE were calculated for the entire held out subset set as well as separately per region as illustrated in Fig. 3.

$$R^2 = 1 - \frac{\sum (SOC_o - SOC_p)^2}{(SOC_o - \overline{SOC_o})^2} \tag{4}$$

$$RMSE = \sqrt{\frac{\sum (SOC_o - SOC_p)^2}{N}} \tag{5}$$

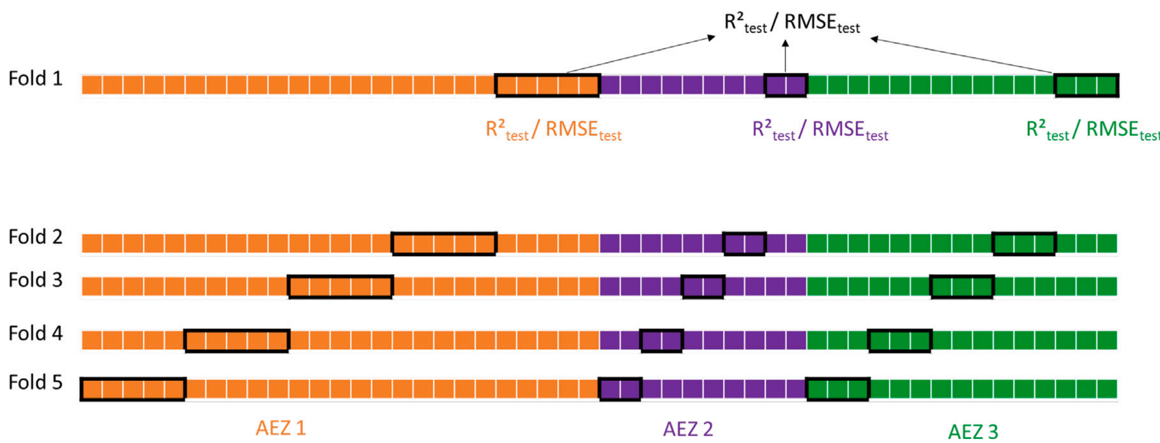

Fig. 3. Schematic representation of the 5-fold cross-validation, where for each fold metrics are calculated on the complete held-out set as well as for each Agro-ecological zone (AEZ). The colored squares depict the calibration data, the test set varies for each fold as indicated by the black borders.

The hyperparameters *max_samples* and *max_features* were kept consistent across models to enable a fair comparison between the models. Specifically, the fraction of features considered at each split *max_features* was fixed at 20%, ensuring consistency despite differences in the total number of available predictors. The choice of setting *max_samples* to 20% was similarly pragmatic and served to maintain an effective level of bootstrap aggregation ("bagging") among the parallel regression trees. The number of estimators was set to 100. A randomized grid-search hyperparameter optimization did not lead to significant improvements in model performance. Other hyperparameters were set to their default values in the *RandomForestRegressor* function.

2.6. Validation

The validation was done by calculating the R^2, RMSE, RPIQ (Ratio of performance to inter-quartile distance) and bias over the validation set for the MODEL_MAP. The validation metrics were also calculated separately for each region to evaluate the applicability of the model at smaller scale. The RPIQ was calculated as the ratio of the RMSE on the validation set to the interquartile range (IQR) of the validation set (Eq. (6)), the bias as calculated as the mean of the observed residuals (Eq. (7)).

$$RPIQ = \frac{RPIQ}{IQR} \tag{6}$$

$$Bias = \frac{\sum(SOC_o - SOC_p)}{N} \tag{7}$$

2.7. Model interpretation

To interpret the importance and contribution of the selected features in the MODEL_MAP, SHapley Additive exPlanations (SHAP) values were calculated using the SHAP package in Python (Lundberg et al., 2020). SHAP values are based on cooperative game theory and represent the contribution of each feature to the prediction for each observation. The sum of the SHAP values for each feature for a given prediction give the deviation of the prediction to the global mean. The SHAP values of five selected fields were visualized to interprete the contribution of spectral and geographical features to the predictions. The relation between each feature and its SHAP value was visualized using dependence plots.

2.8. Uncertainty estimation

The uncertainty of the predictions was assessed by fitting a quantile regression forest (QRF) using the selected features after cross-validation. QRFs are a modification of random forests that allow to estimate the conditional distribution of the dependent variable (Meinshausen and Ridgeway, 2006). The sklearn_quantile v0.0.29 package for Python was used to fit the QRF models. The quantiles were validated calculating the Quantile Coverage Probability (QCP), the proportion of observation in the test data below each estimated quantile, on the test data. Prediction intervals at level 30%, 40%, 50%, 60%, 70%, 80% and 90% were validated on the test set by calculating the Prediction Interval Coverage Probability (PICP), i.e. the percentage of observations in the test set that are within the calculated prediction interval at each PI level. The PICP was used to assess the validity of the uncertainty intervals while the QCP was used to detect asymmetry in the uncertainty estimation (Tian et al., 2024).

2.9. Spatial averages and uncertainty

The value of the obtained SOC content map for regional monitoring was assessed by estimating the average SOC content and its uncertainty for five soil regions, proposed for soil monitoring, in the Walloon region. These regions were defined to represent homogeneous areas in terms of soil properties in the context of the upcoming EU 'Soil Monitoring Law' (European Commission, 2023). The five soil regions show strong similarities to the previously defined AEZs (Fig. 2).

The standard error of the predictions was estimated as the standard deviation of 1000 simulations from the conditional distribution of a prediction using the ranger package in R (Wright et al., 2024). The package allows to simulate values from the conditional distribution, estimated by the QRF model, of the predictions through the predict function, passing `what = function(x) sample(x, 1000, replace=TRUE)`. Consequently the residuals of the validation dataset were standardized by dividing them by the standard error of the predictions. A variogram model was then fitted to the standardized residuals using the gstat package in R (Gräler et al., 2016; Pebesma, 2004). Finally, the standard error of the spatial average is estimated by monte-carlo integration. For each of the five soil regions, 10,000 random pairs of fields are drawn, with replacement. For each pair, the correlation of the standardized residuals is calculated using the variogram model, and multiplied with both standard errors of the predictions of both fields, resulting in a covariance estimate. Finally, the standard error of the spatial average is estimated as the mean of the 10,000 covariances (Wadoux and Heuvelink, 2023).

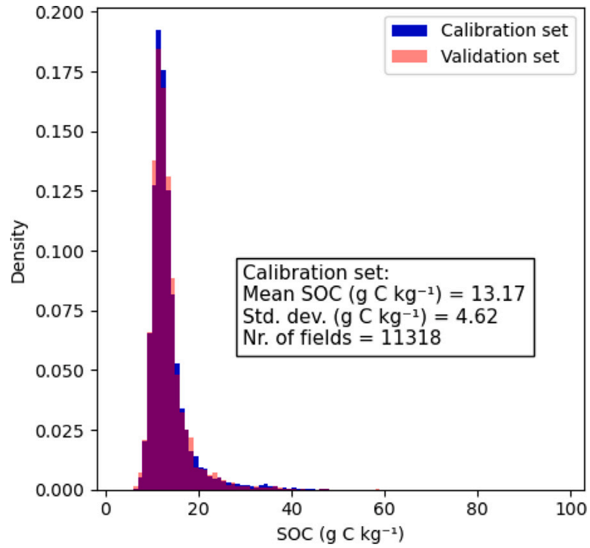

Fig. 4. Distribution of the Soil Organic Carbon (SOC) content in calibration and validation set.

3. Results

3.1. Descriptive statistics

The calibration data has a mean SOC content of 13.17 g C kg^{-1} with a standard deviation of 4.62 g C kg^{-1}. The random split ensured a similar SOC content distribution in the calibration and validation data (Fig. 4). Furthermore, we can assume that SOC content at parcel-level remains stable during the three years included in the dataset. This is supported by data from 30 fields that were analyzed in 2018 and 2021, for which the mean absolute difference in SOC content was 0.71 g C kg^{-1}, yet the mean difference between both years is 0.006 g C kg^{-1} suggesting that the difference in SOC content between years is mostly influenced by random error in the measurements.

3.2. Model comparison

The range of R^2 and RMSE values for the three different models in cross-validation are given in Fig. 5. The figure visualizes the performance of the three sets of predictors, on the entire training dataset, as well as the R^2 (Fig. 5(a)) and RMSE (Fig. 5(b)) when evaluating the same models separately on the Loam Belt and the Condroz regions. The SPEC+GEO model, evaluated over the Walloon region, results in R^2 = 0.57–0.64 and RMSE = 2.65–2.96 g C kg^{-1}. The SPEC model reaches R^2 = 0.35–0.44 and RMSE = 3.19–3.63 g C kg^{-1}, while the GEO model reaches R^2 = 0.45–0.53 and RMSE = 3.06–3.34 g C kg^{-1}. For the Loam Belt the GEO model yields an R^2 of 0.04–0.07, the SPEC model has R^2 of −0.04–0.1, while the SPEC+GEO model yields R^2 = 0.25–0.31. In the Condroz region, the R^2 ranges are 0.02–0.06, 0.13–0.28 and 0.31–0.37 for the GEO, SPEC and SPEC+GEO model respectively. Since RFE was applied for each fold in cross-validation, each fold can result in a different set of selected features. The frequency of selection across folds is shown in Table 2, only the most frequently selected features are shown.

3.3. Validation and interpretation

Considering the results of the model comparison and feature selection algorithm, a set of features is selected for calibrating a Random Forest model that is then validated on the validation dataset, this model is referred to as MODEL_MAP. The selected features are:

Table 2
Selection frequency of the most selected features in cross-validation for the model with spectral features (SPEC) and the model with spectral and environmental features (SPEC+GEO). Acronyms: AEZ: Agro-Ecological Zone, NDBXBY denotes the normalized difference of bands X and Y.

Feature	Selection frequency (SPEC)	Selection frequency (SPEC + GEO)
Fine fraction content	–	100%
Elevation	–	100%
AEZ	–	100%
NDB5B11	100%	100%
NDB11B12	100%	100%
NDB2B3	100%	100%
B4	80%	100%
NDB4B11	60%	40%
NDB3B11	80%	40%
B3	80%	0%
NDB6B11	60%	0%
B12	60%	0%
NDB8AB11	60%	0%
…	…	…

Table 3
Validation metrics by AEZ of MODEL_MAP.

Validation dataset	Samples in validation data	R^2	RMSE (g C kg^{-1})	Bias (g C kg^{-1})	RPIQ
All	2854	0.56	2.72	−0.09	1.10
Limoneuse	1946	0.26	2.56	−0.07	0.95
Condroz	395	0.36	2.76	0.03	1.45
Fagnes-Famenne	74	0.35	4.30	−0.30	1.57
Ardennes	36	0.27	5.28	1.07	1.94

- AEZ
- Fine fraction content
- Elevation
- NDB2B3
- NDB11B12 (=NBR2)
- NDB5B11
- B4

For model interpration, NDB2B3 and NDB5B11 are multiplied by −1, to obtain NDB3B2 and NDB11B5 since having positive values for the spectral indices makes them easier to interpret. The performance of this model on the test set is shown in Fig. 6. The model yiels R^2 = 0.56, RMSE = 2.72 g C kg^{-1} and RPIQ = 1.11. The color of the points shows the corresponding AEZ. A more elaborate validation is shown in Table 3, with performance metrics of the model within the largest AEZs to evaluate its local performances. The model is consequently used for mapping SOC over all parcels in the Walloon region.

Using QRF, prediction intervals were calculated at different levels (30%, 40%, 50%, 60%, 70%, 80% and 90%). The PICP, calculated on the test set, is visualized in Fig. 7(a). Points above the 1:1 line indicate there is a conservative estimation of uncertainty, while points below the 1:1 line indicate an underestimation of uncertainty. The QCP is a validation of the estimated quantiles and allows to detect asymmetry in the interval coverage (Fig. 7(b)). Points above the 1:1 are an indication that quantiles are overestimated.

The SOC content estimations are shown for an area in the Limoneuse region in Fig. 8. Fig. 8(a) shows the SOC content predictions and associated uncertainty (PIR) of a model with the three geographic covariates. Fig. 8(b) shows the predictions of a model with the four selected spectral indices, and Fig. 8(c) shows the predictions of MODEL_MAP. The complete SOC content map is shown in Fig. 9. For five parcels, selected to cover different contexts, waterfall plots show the SHAP value for each variable. A large SHAP value means that this variable has a large contribution in explaining the deviation of the predicted SOC content from the global mean. Adding all SHAP values for a prediction with the global mean results in the predicted SOC content. Fig. 10 gives

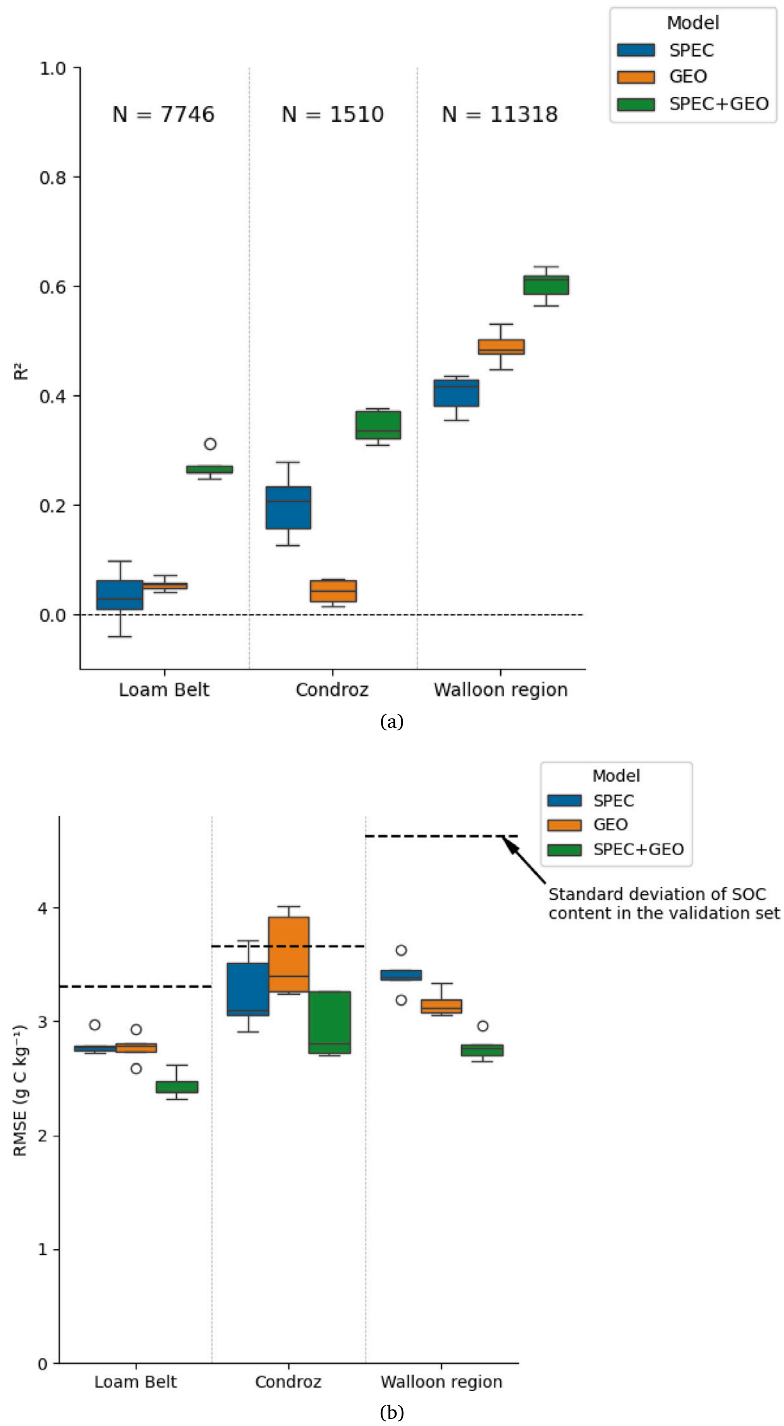

Fig. 5. Comparison of the R^2 (a) and RMSE (b) for three models trained on different sets of features: spectral features (SPEC), environmental features (GEO), and combined features (SPEC+GEO) in 5-fold cross-validation.

the SHAP partial dependence plot, showing the SHAP value of each variable in relation to the value of the variable.

3.4. Spatial aggregation

An exponential variogram model was fitted to the standardized residuals of the validation set. The fitted variogram model has the following parameters; nugget: 0.43, sill: 0.78 and range: 679 m (Fig. 11). The result of Monte Carlo integration of the variance of the spatial averages for five soil regions is shown in Table 4. This table shows the average SOC content per soil region and its standard error for each soil region, together with the number of parcels in each soil region and the average standard error of the predictions at parcel-level.

4. Discussion

4.1. Model comparison

The results of model comparison show that both spectral and geographic covariates are relevant to explain SOC content variation in

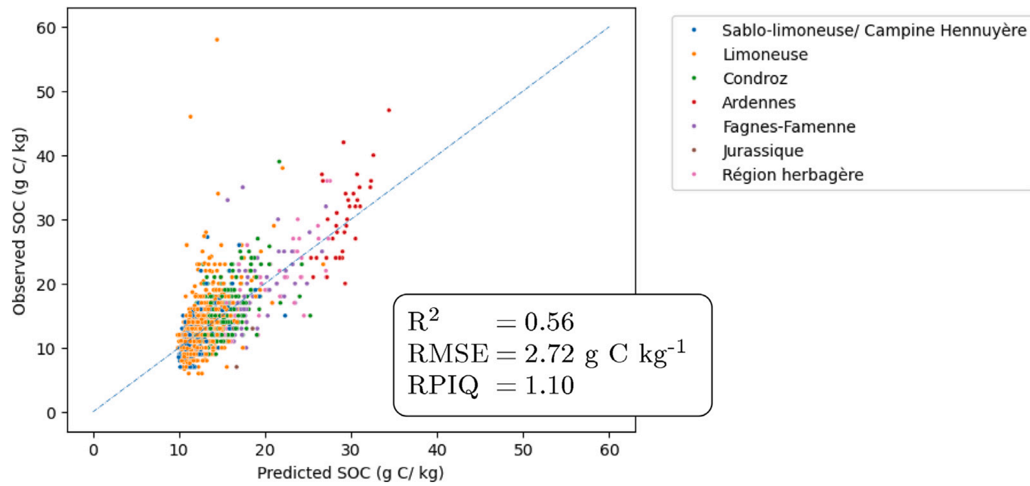

Fig. 6. Predicted SOC content vs. observed SOC content in the test data for the MODEL_MAP.

Table 4
Estimates and standard error of the average Soil Organic Carbon (SOC) content for soil regions.

Soil region	Nr. of parcels	Parcel-level	Aggregated level	
		Avg. Std. error (g C kg^{-1})	$\overline{SOC_{pred}}$ (g C kg^{-1})	Std. error (g C kg^{-1})
Loam belt	56,404	2.83	12.64	0.004
Condroz	7756	3.35	15.16	0.011
Fagnes-Famenne	2888	5.26	18.80	0.046
Ardennes	5306	6.89	30.02	0.029
Jurassique	1135	6.10	17.01	0.138

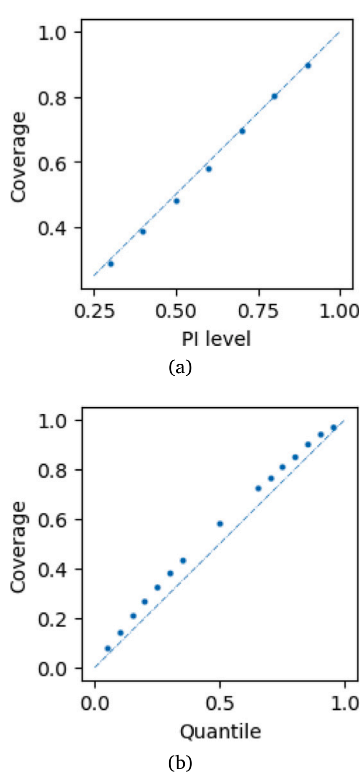

Fig. 7. Validation of the estimated quantiles: Prediction Interval Coverage Probability (a) and Quantile Coverage Probability (b). The Prediction Interval level (PI level) represents the nominal coverage probability of the prediction interval.

the Walloon region. Based on cross-validation results over the Walloon region, the combined model (SPEC+GEO, R^2: 0.57–0.64 and RMSE: 2.65–2.96 g C kg^{-1}) outperforms the models based on only spectral (SPEC, R^2: 0.35–0.44 and RMSE: 3.19–3.63 g C kg^{-1}) or geographic (GEO, R^2: 0.45–0.53 and RMSE: 3.06–3.34 g C kg^{-1}) predictors, indicating that both sources of information are complementary. Moreover, the combined (SPEC+GEO) model shows better performance within AEZS. The SOC content variability in the Loam Belt, characterized by intensive agriculture and low SOC content variability, is poorly explained by the SPEC and GEO models, with R^2 close to 0. The combined model (SPEC+GEO) reaches an R^2 of 0.25–0.31 illustrating that the combination of features allows to better explain SOC variation within the more homogeneous AEZs. A slightly different pattern is observed in the Condroz region, where the SPEC model performs better than the GEO model. Still the combined model outperforms both models, reaching an R^2 of 0.31–0.38. This also indicates that contextual information is needed for a model based on spectral predictors to explain local SOC content variation. Possibly, the environmental covariates explain spatial trends in SOC content at larger scales, due to the trends in texture, elevation and climate. The spectral signal could then allow to capture local variation in SOC, conditional on the information gained from the environmental covariates. It is also possible that the combination of predictors improves the model because of an interaction effect between the spatial covariates and the spectral signal, for example through the effect of soil texture on soil reflectance (Nocita et al., 2014). These results confirm that in the context of the Walloon region, a regional SOC prediction model improves by adding contextual information and thus allows the model to adapt to the different local conditions. This is in line with other findings (Broeg et al., 2024; Nocita et al., 2014; Safanelli et al., 2020).

For future studies, a comparison of the added value of bare soil spectral features to a more elaborate DSM approach in the Walloon region would be interesting. Such analysis was done by Vanongeval et al. (2024) for the Flanders region (Belgium). A hybrid model consisting of spectral and environmental covariates was also observed to outperform the traditional DSM model.

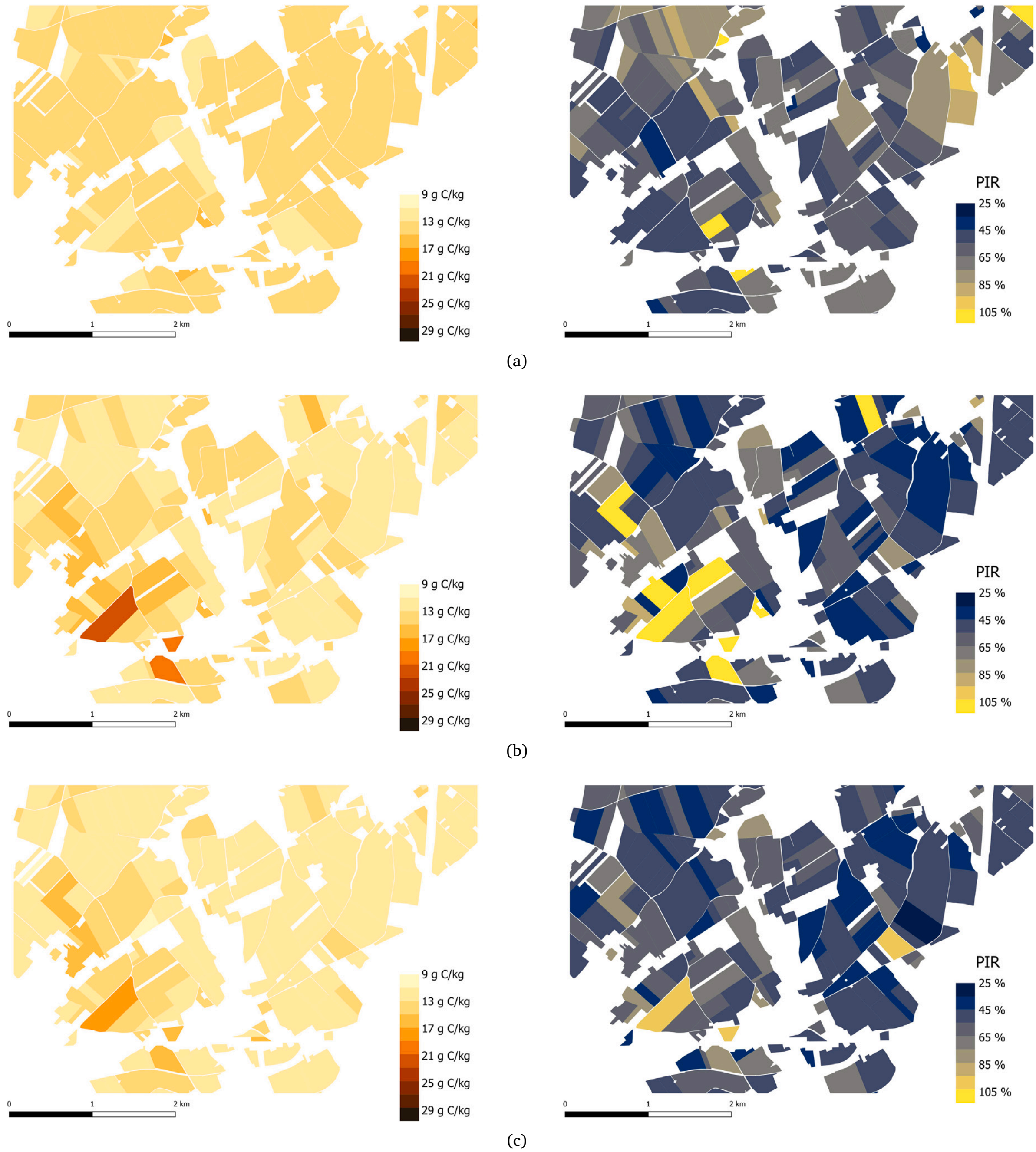

Fig. 8. Zoom on the predictions and Prediction Interval Ratio (PIR) of three models (geographic covariates (a), spectral covariates (b) and MAP_MODEL (c)).

4.2. Validation

On the validation set, MODEL_MAP can predict SOC content with an RMSE of 2.70 g C kg^{-1}. For samples in the Limoneuse region only, the RMSE is 2.56 g C kg^{-1} due to the smaller variability in SOC contents in the region. On the contrary, in the Fagnes-Famenne and Ardennes the RMSE is higher (4.30 and 5.8 g C kg^{-1}) respectively. Since the R^2 is larger than 0 within each region, the model does not only explain large-scale spatial trends but also explains part of the SOC variability within the more homogeneous AEZs. Importantly, the estimated quantiles are validated on the test set, with a PICP close to the nominal level (Fig. 7(a)). The QCP is also close to the 1:1 line (Fig. 7(b)). The uncertainty estimation is thus valid and can be used to assess the uncertainty of predictions at parcel-level.

The performance of MODEL_MAP can be compared to previous studies in the Walloon region. A model trained on the lab spectra of the European LUCAS data and validated on 61 points in the Walloon region reached an RMSE of 3.2 g C kg^{-1} (R^2 = 0.6) (Castaldi et al., 2018). The same model validated exclusively on points located in the Loam Belt reached an RMSE of 1.2 g C kg^{-1} (R^2 = 0.6). Therefore, the model on continuous lab spectra has a similar performance over the Walloon region yet has higher accuracy within the Loam Belt as compared to the Sentinel-2 based SOC content prediction model. A local PLSR model on a spectral library for the Walloon region was reported to predict SOC content with an RMSE of 1.3 g C kg^{-1} and R^2 of 0.92 (Genot et al., 2011). At larger spatial scales, the R^2 of models on lab spectra is larger due to the larger variation in SOC content. Yet, the RMSE is the same range as what has been obtained for field predictions in

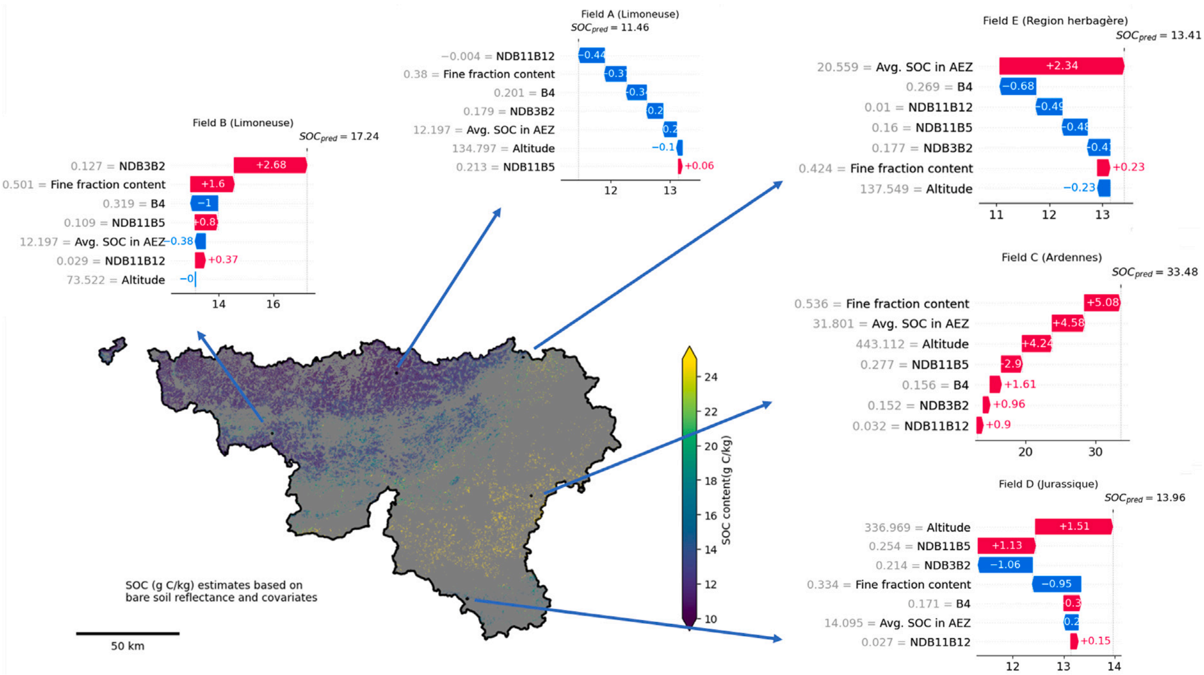

Fig. 9. SOC content predictions over the Walloon region by the optimal model. Waterfall plots show the SHAP values for five parcels, which explain the difference of the predicted SOC content to the global mean (13.14 g C kg^{-1}).

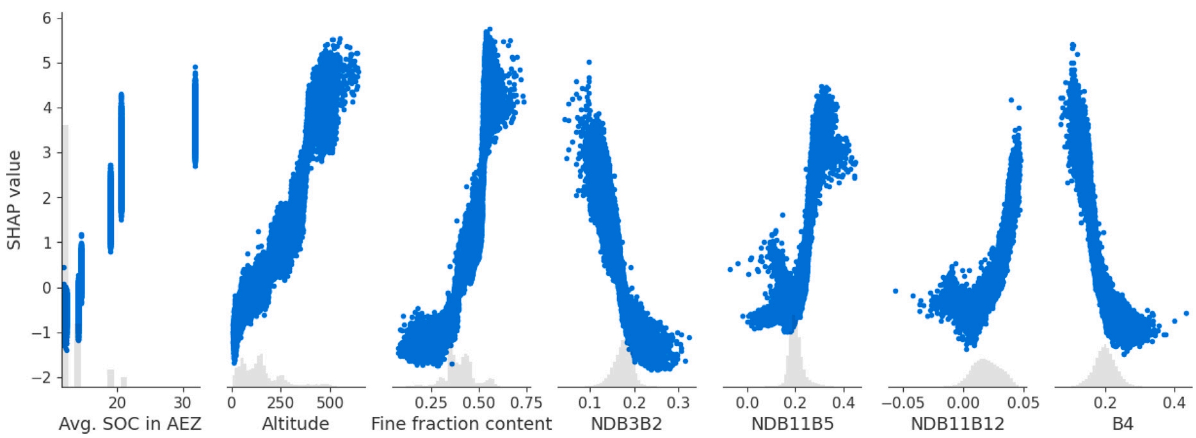

Fig. 10. SHAP partial dependence plot, showing the relation between the predictors' values and their corresponding SHAP values.

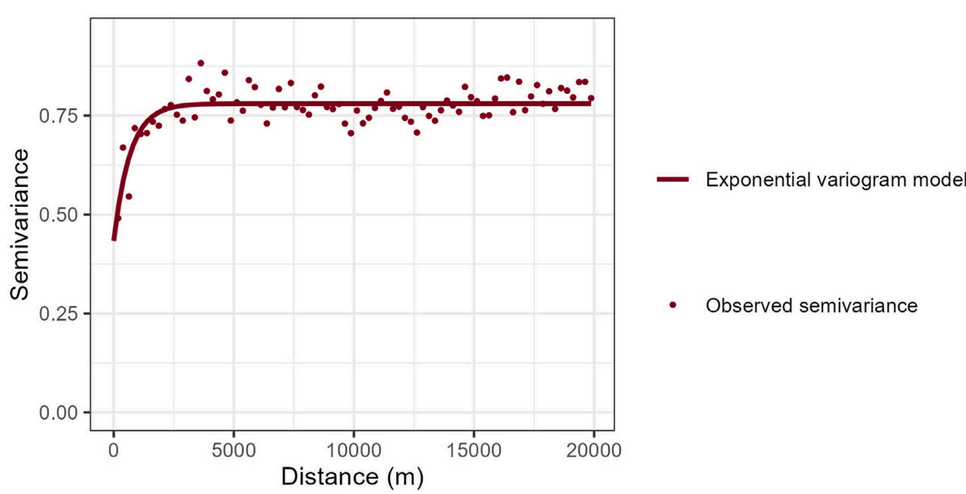

Fig. 11. Semivariance of the standardized residuals, calculated on the validation set, with fitted exponential variogram model.

this Sentinel-2 based study. In the study by Nocita et al. (2014), an R^2 of 0.84 on croplands in Europe coincides with an RMSE of 3.6 g C kg^{-1}. Stevens et al. (2013) reported a performance in the same range, with a model for Europe reaching an R^2 of 0.79 and an RMSE of 4.0 g C kg^{-1}. The Sentinel-2-based predictions reported in this study are therefore in line with expectations and large improvements in accuracy by adding predictors or training data are not expected. There is no increase in accuracy when predicting the average SOC content at field level compared to previous studies at point support using the LUCAS database. A possible reason is that there is larger uncertainty in the training data when working with composite samples of a larger support. On the other hand, the gain in accuracy in the Walloon region would be limited since the SOC content variation within the field is of the same magnitude as SOC content variation within a 4 m radius (Goidts et al., 2009). In different contexts, the SOC variability at parcel level may be larger, therefore allowing a larger increase in accuracy from pixel to field level (Lagacherie et al., 2024).

Other remote-sensing based models in the Walloon region have reported poor results when restricted to areas with low SOC content variation (Castaldi et al., 2019). The model in Dvorakova et al. (2023), a PLSR model with reflectance of the 10 Sentinel-2 bands as predictors, was validated at parcel level over the Walloon region. The standard deviation of the residuals is of 2.8 g C kg^{-1} yet with a mean error (bias) of 0.7 g C kg^{-1} and on a database with a standard deviation of 3.2 g C kg^{-1}. These studies show that the SOC content variation in the Walloon region is close to the accuracy of SOC predictions based on multispectral remote-sensing data.

SOC content mapping can also be done with a DSM approach, modeling SOC content with a set of soil forming factors as predictors. This approach has allowed to map SOC content at field-level for croplands in the Walloon region with an RMSE of 3.2 g C kg^{-1}, and thus a higher, but comparable uncertainty to the predictions based on multispectral satellite data (Zhou et al., 2022). The performance of the obtained SOC prediction model is thus comparable to results in existing literature on SOC content mapping in the Walloon region. Given the accuracy obtained on continuous spectra of dried and crushed samples, this is likely close to be the highest attainable accuracy using multispectral data. This is further supported by a general review of SOC content mapping with remote sensing. It has been observed that the RMSE is dependent on the standard deviation of SOC contents in the study area. For a standard deviation of 4.9 g C kg^{-1}, the expected RMSE of a SOC content model is around 3.7 g C kg^{-1} (Vaudour et al., 2022). Besides, the accuracy of the model is also limited by the uncertainty in the calibration and validation data. Soil sampling of a field for routine fertility analysis is prone to errors. The standard deviation for repeated sampling the same field was estimated at 0.8 g C kg^{-1} (CV = 8%) for croplands in the Belgian Loam Belt, while the standard deviation of repeated laboratory analysis using the Walkley & Black method was between 1.1 and 1.4 g C kg^{-1} (Goidts et al., 2009; Walkley and Black, 1934).

4.3. Mapping and model interpretation

The obtained SOC content map reflects the known positive trend in SOC content from North to South which is correlated to trends in elevation, soil type and climate (Chartin et al., 2017). At smaller distances, the identified spectral indices are relevant to model SOC content variability as is illustrated for a selection of five fields in Fig. 9. In the Limoneuse region, SOC contents lower than average are predicted. For field A, the NDB11B12 has a strong contribution to the prediction of 11.46 g C kg^{-1}. For field B, on the other hand, a SOC content of 17 g C kg^{-1} is predicted where mostly NDB3B2 and the fine fraction content contribute to this prediction, which is higher than the global average. For field C, in the Ardennes, a higher SOC content than average is predicted (Fig. 9). This is mostly explained by the higher fine fraction content, higher elevation and higher average SOC in the region but also the spectral features contribute positively to the predicted SOC content. For field D, in the Jurassique region, the summed contribution of the spectral features is small and the predicted SOC content is a result of the contribution of altitude and the fine fraction content. The prediction of field E is lower than the average in its respective agricultural region, with all four spectral predictors contributing negatively to the SOC content prediction. The five selected fields show that in different contexts, different predictors have relevance for SOC content predictions, with both spectral and geographical predictors having important contributions.

The relation between predictors and predicted SOC content can be further interpreted using SHAP partial dependence plots (Fig. 10). As the NDB3B2 index (Band 2: 490 nm and band 3: 560 nm) increases, the expected SOC content decreases (Fig. 10). This indicates a possible absorption feature in the visible range, associated with SOC content meaning that higher SOC content causes increased absorption in band 3 or decreased absorption in band 2. Previous studies have observed absorption at 600 nm in samples with increasing SOC content (Bartholomeus et al., 2008; Nocita et al., 2014; Shi et al., 2020). Ben-Dor et al. (1997) observe a decrease in slope between 450 nm and 638 nm during the decomposition of organic matter and attribute this to the breakdown of chlorophyll. It is likely that absorbance around 600 nm explains the importance of the normalized difference of band 2 and 3 in the models. Fig. 12 shows the average spectra for different SOC content classes, of all LUCAS 2015 samples on agricultural land in Belgium (European Commission. Joint Research Centre., 2020). After continuum removal, there is a clear absorption feature around 600 nm, which might affect reflectance in band 3. The reflectance spectra of the LUCAS database also show that the slope in the visible range is smaller for higher SOC contents, possibly explaining the importance of NDB2B3.

The normalized difference of band 11 and 12 (=NBR2) is selected consistently by the feature elimination algorithm. Absorption by lignin and cellulose has an absorption peak at 2100 nm, i.e. the lower range of band 12, possibly explaining the correlation of the NBR2 index with SOC content (Nagler et al., 2003). Yet the NBR2 is also affected by soil moisture and an absorption feature by clay minerals in band 12 (Fig. 12) (Viscarra Rossel et al., 2011; Viscarra Rossel and Behrens, 2010). It is likely that in the context of the Walloon region, the NBR2 serves as an indicator of the trend in clay content and/or moisture regime, which are in turn correlated to SOC content due to their effect on the stability of SOM. Besides, this raises concerns in using the NBR2 for developing the bare soil composite since parcels with high SOC or clay content may be masked incorrectly. Karlshoefer et al. (2025) propose an adaptive NBR2 filter to avoid such problems. Yet this does not avoid the issue that the NBR2 is associated to SOC content through indirect pathways and will thus may not be able to explain temporal SOC content changes.

The NDB11B5 is also associated to SOC content. A possible explanation is absorption in the red-edge region of band 5, although no knowledge of absorption features in this spectral range by organic matter. Dodin et al. (2021) show that the NDB11B8 A and NDB11B4 react to the application of organic amendments due to a stronger decrease in reflectance in the red-edge bands as compared to band 11. There is however no clear physical explanation for the importance of NDB11B5 in the SOC content prediction model. Also the reflectance in band 4 was selected in the MODEL_MAP. This can be explained by the general decrease in reflectance with increasing organic matter. However, Fig. 12 shows that in the spectral region of band 4 (665 nm), specific absorption by organic matter may also occur.

While literature indicates absorption by OM between 1500 nm and 1800 nm, the LUCAS soil samples show no differences between the SOC content classes in the region of band 11 (Fig. 12) (Viscarra Rossel and Behrens, 2010; Demattê et al., 2015).

In previous studies, SOC prediction has often been done by using only the 10 reflectance values (Broeg et al., 2024; Dvorakova et al., 2023; Vanongeval et al., 2024). We observe that prediction models

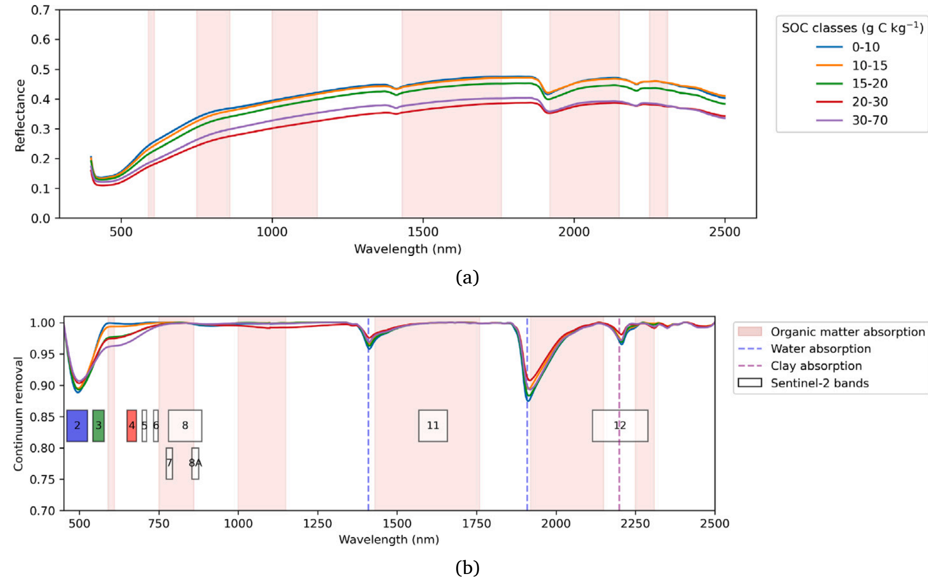

Fig. 12. Reflectance (a) and continuum-removed reflectance (b) averaged per SOC content class, for samples in Belgium on agricultural land of the 2015 LUCAS campaign. The spectral bands of the optical sensor on board the Sentinel-2 satellites. Regions sensitive to absorption by organic matter and absorption features by soil water and clay minerals are shown.

can be improved by considering spectral indices. The indices identified in this paper can serve as a starting point when data availability is limited. When applying machine-learning algorithms, there is a risk of overfitting because of the presence of autocorrelation in the data (Wadoux et al., 2020). Therefore, it is relevant to understand the physical explanation between the spectral features and SOC content to assess the potential transferability of the model.

4.4. Applications

4.4.1. SOC monitoring at parcel-level

Accurate estimation of SOC content by remote sensing may allow for monitoring temporal SOC content changes. This requires to compare the precision of the estimates to the expected SOC content change. In Poeplau and Don (2015), a global meta-analysis of field experiments shows an average carbon sequestration of 320 kg C ha^{-1} yr^{-1} when implementing cover crops. In Launay et al. (2021), a model-based approach estimates a carbon sequestration rate of 131 kg C ha^{-1} yr^{-1} when implementing cover crops, or 184 kg C ha^{-1} yr^{-1} when combining it with improved nutrient recycling. Given these estimates, a constant net carbon sequestration rate of 300 kg C ha^{-1} yr^{-1} provides a rough estimate of the carbon sequestration under improved management. It is considered that this input is supplied to the first 30 cm of a soil with a bulk density of 1.5 g cm^{-3}, an increase of 1 g C kg^{-1} can be achieved over 15 years.

Given the precision of the map, validated on farmer routine soil analyses, the SOC content estimation at field level has an RMSE of 2.57 g C kg^{-1} in the Loam Belt (Table 3). Assuming two maps with a precision of 2.5 g C kg^{-1}, the MDD equals 12.4 g C kg^{-1} for a power of 0.8, at a tolerance level of 0.05, and assuming that there is no correlation between the residual error in both maps for the same location. This MDD is insufficient to detect SOC content changes which are attainable in 10 years, as a realistic SOC increase over 10 years is around 1 g C kg^{-1} under a net carbon sequestration rate of 300 kg C ha^{-1} y^{-1}. Despite being approximate calculations, the results indicate that multispectral data is not suitable for SOC monitoring at parcel-level, in time frames smaller than 50 years. Multispectral satellite data is thus rather suited as a tool for SOC mapping, than for SOC monitoring at parcel-level.

The growth of voluntary carbon markets has created an interest in accurately measuring SOC stock changes at parcel-level. This has proven to be challenging, even with soil sampling, because of within-field variability and the slow build-up of SOC. For the assessment of SOC stock changes, a sampling density of 1.2 ha sample^{-1} is not sufficient to accurately estimate SOC stock changes after 5–10 years of regenerative practices (Bradford et al., 2023). Therefore, there is a high cost associated to quantifying SOC changes at field-level, and it may be worth to rather estimate the average effect for a soil conservation project over multiple fields. Bradford et al. (2023) show that when jointly assessing SOC stock change on 30 field pairs, the average effect is estimated within ±1 Mg C ha^{-1} using a sampling density of 1.2 ha sample^{-1}. Given the accuracies of remote sensing-based estimates, the same rationale should be applied. The SOC maps offer information on the spatial SOC variability and given that estimates are available at parcel-level, the SOC maps offer the opportunity to compare groups of fields, with different management practices, in comparable environments.

4.4.2. SOC mapping at regional level

The variogram indicates that the autocorrelation of the residuals is only present at small distances, with a range of 679 m this is only relevant for adjacent fields. The nugget effect indicates that most of the residual variation is due to random model or measurement errors.

The Monte Carlo integration allows to estimate the uncertainty on the average for any spatial grouping unit. As expected, the standard error is strongly reduced when assessing the average SOC content for soil regions compared to individual parcels. The uncertainty of the spatial average is influenced by the number of fields in the grouping unit, the variability within the unit, the uncertainty of predictions in the unit and the geographic position of the fields. The standard error of the average SOC content for soil regions is between 0.004 g C kg^{-1} and 0.138 g C kg^{-1} (Table 4). The standard error is smallest for the Loam Belt, which has the largest number of fields (56,404) and smaller uncertainty at parcel-level. The standard error is largest for the Jurassique, which has the smallest number of fields (1135) and a higher uncertainty on the estimates at parcel-level.

Our results illustrate that there is value in SOC content maps for regional SOC content monitoring. When the training data is not guaranteed to represent a random sample, training a model to map SOC content over the region can allow obtaining a spatial average with a high precision for any spatial unit. With access to the SOC content predictions and standard errors at parcel-level and the fitted variogram model, other users can estimate the average SOC content and its uncertainty for any spatial unit of interest. For example, with access to a database of fields where soil conservation practices have been applied, the average SOC content of these fields can be compared to a set of control fields with estimates of uncertainty. This does not require access to the original soil analyses, but only to the SOC content estimates and associated standard error at parcel-level and the fitted variogram model. Such approach can thus be used for flexible frameworks SOC monitoring without the need to share potentially sensitive information. This may also be valuable in frameworks of soil health monitoring, where soil health indicators will be monitored at regional scale (European Commission, 2023).

5. Conclusion

We observe that in the context of the Walloon region, with a high availability of data at the parcel level a random forest model on spectral information yields satisfactory results for SOC mapping when combined with a limited set of environmental covariates. Therefore, a multispectral bare soil composite is useful but complementary to spatial covariates for SOC mapping. Furthermore, spectral indices relevant to SOC mapping were identified. The spectral features important for explaining spatial SOC variation are the normalized difference of various Sentinel-2 bands and the absolute reflectance in the red band (band 4). The selection of these features can be explained by known absorption features of organic matter at 600 nm, 700 nm and 2200 nm as well as the effect of organic matter on the albedo of the soil. The obtained map has a higher spatial resolution than existing SOC maps of the Walloon region with a slightly higher accuracy. The obtained model predicts SOC content at parcel-level over the Walloon region with an RMSE of 2.7 g C kg^{-1}. Given the accuracy of the model used for SOC mapping, it is not expected that multispectral satellite data can be used for SOC monitoring at parcel-level. SOC content maps obtained via remote sensing can, however, play a role for regional SOC monitoring, with the uncertainty on the aggregated average depending on the size of the spatial unit, the degree of autocorrelation and the uncertainty of the model at point support.

CRediT authorship contribution statement

Dries De Bièvre: Writing – original draft, Methodology, Formal analysis, Data curation, Conceptualization. **Pierre Defourny:** Writing – review & editing, Supervision, Conceptualization. **Bas van Wesemael:** Writing – review & editing, Supervision, Funding acquisition, Conceptualization.

Declaration of competing interest

The authors declare that they have no known competing financial interests or personal relationships that could have appeared to influence the work reported in this paper.

Acknowledgments

The authors thank the "Plan de Relance de la Wallonie, Belgium" for financing this research under convention number O3.02.05-22-5153. They also thank the REQUASUD network of soil laboratories for the availability of reference soil data (licence number A07/2021). The LUCAS 2015 topsoil dataset used in this work was made available by the European Commission through the European Soil Data Centre managed by the Joint Research Centre (JRC), http://esdac.jrc.ec.europa.eu/.

Data availability

The authors do not have permission to share data.

References

Bartholomeus, H.M., Schaepman, M.E., Kooistra, L., Stevens, A., Hoogmoed, W.B., Spaargaren, O.S.P., 2008. Spectral reflectance based indices for soil organic carbon quantification. Geoderma 145 (1), 28–36. http://dx.doi.org/10.1016/j.geoderma.2008.01.010.

Ben-Dor, E., Inbar, Y., Chen, Y., 1997. The reflectance spectra of organic matter in the visible near-infrared and short Wave Infrared Region (400–2500 Nm) during a controlled decomposition process. Remote Sens. Environ. 61 (1), 1–15. http://dx.doi.org/10.1016/S0034-4257(96)00120-4.

Beven, K.J., Kirby, M.J., 1979. A physically based, Variable Contributing Area model of basin hydrology / un modèle à base physique de zone d'appel variable de l'hydrologie du bassin versant. Hydrol. Sci. Bull. 24 (1), 43–69. http://dx.doi.org/10.1080/02626667909491834.

Biney, J.K.M., Saberioon, M., Borůvka, L., Houška, J., Vašát, R., Chapman Agyeman, P., Coblinski, J.A., Klement, A., 2021. Exploring the suitability of UAS-based multispectral images for estimating soil organic carbon: Comparison with proximal soil sensing and spaceborne imagery. Remote. Sens. 13 (2), 308. http://dx.doi.org/10.3390/rs13020308.

Bradford, M.A., Eash, L., Polussa, A., Jevon, F.V., Kuebbing, S.E., Hammac, W.A., Rosenzweig, S., Oldfield, E.E., 2023. Testing the feasibility of quantifying change in agricultural soil carbon stocks through empirical sampling. Geoderma 440, 116719. http://dx.doi.org/10.1016/j.geoderma.2023.116719.

Breiman, L., 2001. Random forests. Mach. Learn. 45 (1), 5–32. http://dx.doi.org/10.1023/A:1010933404324.

Broeg, T., Don, A., Wiesmeier, M., Scholten, T., Erasmi, S., 2024. Spatiotemporal monitoring of cropland soil organic carbon changes from space. Global Change Biol. 30 (12), e17608. http://dx.doi.org/10.1111/gcb.17608.

Castaldi, F., Chabrillat, S., Chartin, C., Genot, V., Jones, A.R., van Wesemael, B., 2018. Estimation of soil organic carbon in Arable soil in Belgium and Luxembourg with the LUCAS topsoil database. Eur. J. Soil Sci. 69 (4), 592–603. http://dx.doi.org/10.1111/ejss.12553.

Castaldi, F., Hueni, A., Chabrillat, S., Ward, K., Buttafuoco, G., Bomans, B., Vreys, K., Brell, M., van Wesemael, B., 2019. Evaluating the capability of the sentinel 2 data for soil organic carbon prediction in croplands. ISPRS J. Photogramm. Remote Sens. 147, 267–282. http://dx.doi.org/10.1016/j.isprsjprs.2018.11.026.

Chabrillat, S., Ben-Dor, E., Cierniewski, J., Gomez, C., Schmid, T., van Wesemael, B., 2019. Imaging spectroscopy for soil mapping and monitoring. Surv. Geophys. 40 (3), 361–399. http://dx.doi.org/10.1007/s10712-019-09524-0.

Chartin, C., Stevens, A., Goidts, E., Krüger, I., Carnol, M., van Wesemael, B., 2017. Mapping soil organic carbon stocks and estimating uncertainties at the regional scale following a legacy sampling strategy (Southern Belgium, Wallonia). Digital Soil Mapping across the Globe, Geoderma Reg. Digital Soil Mapping across the Globe, 9, 73–86.http://dx.doi.org/10.1016/j.geodrs.2016.12.006,

d'Andrimont, R., Verhegghen, A., Lemoine, G., Kempeneers, P., Meroni, M., van der Velde, M., 2021. From parcel to continental scale – a first European crop type map based on sentinel-1 and LUCAS copernicus in-situ observations. Remote Sens. Environ. 266, 112708. http://dx.doi.org/10.1016/j.rse.2021.112708.

Demattê, J.A.M., Fongaro, C.T., Rizzo, R., Safanelli, J.L., 2018. Geospatial soil sensing system (GEOS3): A powerful data mining procedure to retrieve soil spectral reflectance from satellite images. Remote Sens. Environ. 212, 161–175. http://dx.doi.org/10.1016/j.rse.2018.04.047.

Demattê, J.A., Morgan, C., Chabrillat, S., Rizzo, R., Franceschini, M., Terra, F., Vasques, G., Wetterlind, J., 2015. Spectral sensing from ground to space in soil science: state of the art, applications, potential and perspectives. pp. 661–732.

Dodin, M., Smith, H.D., Levavasseur, F., Hadjar, D., Houot, S., Vaudour, E., 2021. Potential of sentinel-2 satellite images for monitoring green waste compost and manure amendments in temperate cropland. Remote. Sens. 13 (9), 1616. http://dx.doi.org/10.3390/rs13091616.

Dvorakova, K., Heiden, U., Pepers, K., Staats, G., van Os, G., van Wesemael, B., 2023. Improving soil organic carbon predictions from a sentinel–2 soil composite by assessing surface conditions and uncertainties. Geoderma 429, 116128. http://dx.doi.org/10.1016/j.geoderma.2022.116128.

Dvorakova, K., Heiden, U., van Wesemael, B., 2021. Sentinel-2 exposed soil composite for soil organic carbon prediction. Remote. Sens. 13 (9), 1791. http://dx.doi.org/10.3390/rs13091791.

Dvorakova, K., Shi, P., Limbourg, Q., van Wesemael, B., 2020. Soil organic carbon mapping from remote sensing: The Effect of crop residues. Remote. Sens. 12 (12), 1913. http://dx.doi.org/10.3390/rs12121913.

European Commission, 2023. Proposal for a directive on soil monitoring and resilience - European commission. https://environment.ec.europa.eu/publications/proposal-directive-soil-monitoring-and-resilience_en.

European Commission. Joint Research Centre., 2020. LUCAS 2015 Topsoil Survey: Presentation of Dataset and Results.. Publications Office of the European Union, Luxembourg, http://dx.doi.org/10.2760/616084,JRC121325.

Fendrich, A.N., Matthews, F., Van Eynde, E., Carozzi, M., Li, Z., d'Andrimont, R., Lugato, E., Martin, P., Ciais, P., Panagos, P., 2023. From regional to parcel scale: A high-resolution map of cover crops across Europe combining satellite data with statistical surveys. Sci. Total Environ. 873, 162300. http://dx.doi.org/10.1016/j.scitotenv.2023.162300.

Genot, V., Colinet, G., Bock, L., Vanvyve, D., Reusen, Y., Dardenne, P., 2011. Near infrared reflectance spectroscopy for estimating soil characteristics valuable in the diagnosis of soil fertility. J. Near Infrared Spectrosc. 19 (2), 117–138.

Goidts, E., van Wesemael, B., 2007. Regional assessment of soil organic carbon changes under agriculture in Southern Belgium (1955–2005). Geoderma 141 (3), 341–354. http://dx.doi.org/10.1016/j.geoderma.2007.06.013.

Goidts, E., Van Wesemael, B., Crucifix, M., 2009. Magnitude and sources of uncertainties in soil organic carbon (SOC) stock assessments at various scales. Eur. J. Soil Sci. 60 (5), 723–739. http://dx.doi.org/10.1111/j.1365-2389.2009.01157.x.

Google Earth Engine Developers, 2025. Sentinel-2 S2cloudless Tutorial. https://developers.google.com/earth-engine/tutorials/community/sentinel-2-s2cloudless.

Gräler, B., Pebesma, E., Heuvelink, G., 2016. Spatio-temporal interpolation using Gstat. R J. 8 (1), 204–218.

Guo, L.B., Gifford, R.M., 2002. Soil carbon stocks and land use change: A meta analysis. Global Change Biol. 8 (4), 345–360. http://dx.doi.org/10.1046/j.1354-1013.2002.00486.x.

Hawker, L., Uhe, P., Paulo, L., Sosa, J., Savage, J., Sampson, C., Neal, J., 2022. A 30 m global map of elevation with forests and buildings removed. Environ. Res. Lett. 17 (2), 024016. http://dx.doi.org/10.1088/1748-9326/ac4d4f.

Heiden, U., d'Angelo, P., Schwind, P., Karlshöfer, P., Müller, R., Zepp, S., Wiesmeier, M., Reinartz, P., 2022. Soil reflectance composites—improved thresholding and performance evaluation. Remote. Sens. 14 (18), 4526. http://dx.doi.org/10.3390/rs14184526.

Heil, J., Jörges, C., Stumpe, B., 2022. Fine-scale mapping of soil organic matter in agricultural soils using UAVs and machine learning. Remote. Sens. 14 (14), 3349. http://dx.doi.org/10.3390/rs14143349.

Hively, W.D., Lamb, B.T., Daughtry, C.S.T., Shermeyer, J., McCarty, G.W., Quemada, M., 2018. Mapping crop residue and tillage intensity using WorldView-3 satellite shortwave infrared residue indices. Remote. Sens. 10 (10), 1657. http://dx.doi.org/10.3390/rs10101657.

Johansson, E.L., Andersson, E., Fischer, K., 2024. The rush for carbon in farmland: Mapping the emerging voluntary market for soil carbon credits. http://dx.doi.org/10.2139/ssrn.4784440.

Karlshoefer, P., d'Angelo, P., Eberle, J., Heiden, U., 2025. Evaluation framework for the generation of continental bare surface reflectance composites. Geoderma 459, 117340. http://dx.doi.org/10.1016/j.geoderma.2025.117340.

Lagacherie, P., Arregui, M., Fages, D., 2024. Evaluating the quality of soil legacy data used as input of digital soil mapping models. Eur. J. Soil Sci. 75 (2), e13463. http://dx.doi.org/10.1111/ejss.13463.

Lal, R., 2018. Digging deeper: A holistic perspective of factors affecting soil organic carbon sequestration in agroecosystems. Global Change Biol. 24 (8), 3285–3301. http://dx.doi.org/10.1111/gcb.14054.

Launay, C., Constantin, J., Chlebowski, F., Houot, S., Graux, A.-I., Klumpp, K., Martin, R., Mary, B., Pellerin, S., Therond, O., 2021. Estimating the carbon storage potential and greenhouse gas emissions of French arable cropland using high-resolution modeling. Global Change Biol. 27 (8), 1645–1661. http://dx.doi.org/10.1111/gcb.15512.

Lugato, E., Panagos, P., Bampa, F., Jones, A., Montanarella, L., 2014. A new baseline of organic carbon stock in European agricultural soils using a modelling approach. Global Change Biol. 20 (1), 313–326. http://dx.doi.org/10.1111/gcb.12292.

Lundberg, S.M., Erion, G., Chen, H., DeGrave, A., Prutkin, J.M., Nair, B., Katz, R., Himmelfarb, J., Bansal, N., Lee, S.-I., 2020. From local explanations to global understanding with explainable AI for trees. Nat. Mach. Intell. 2 (1), 56–67. http://dx.doi.org/10.1038/s42256-019-0138-9.

McBratney, A.B., Mendonça Santos, M.L., Minasny, B., 2003. On digital soil mapping. Geoderma 117 (1), 3–52. http://dx.doi.org/10.1016/S0016-7061(03)00223-4.

Meinshausen, N., Ridgeway, G., 2006. Quantile regression forests. J. Mach. Learn. Res. 7 (6).

Mzid, N., Castaldi, F., Tolomio, M., Pascucci, S., Casa, R., Pignatti, S., 2022. Evaluation of agricultural bare soil properties retrieval from landsat 8, sentinel-2 and PRISMA satellite data. Remote. Sens. 14 (3), 714. http://dx.doi.org/10.3390/rs14030714.

Nagler, P.L., Inoue, Y., Glenn, E.P., Russ, A.L., Daughtry, C.S.T., 2003. Cellulose absorption index (CAI) to quantify mixed soil–plant litter scenes. Remote Sens. Environ. 87 (2), 310–325. http://dx.doi.org/10.1016/j.rse.2003.06.001.

Nocita, M., Stevens, A., Noon, C., Van Wesemael, B., 2013. Prediction of soil organic carbon for different levels of soil moisture using vis-NIR spectroscopy. Geoderma 199, 37–42. http://dx.doi.org/10.1016/j.geoderma.2012.07.020.

Nocita, M., Stevens, A., Toth, G., Panagos, P., van Wesemael, B., Montanarella, L., 2014. Prediction of soil organic carbon content by diffuse reflectance spectroscopy using a local partial least square regression approach. Soil Biol. Biochem. 68, 337–347. http://dx.doi.org/10.1016/j.soilbio.2013.10.022.

Padarian, J., McBratney, A.B., 2023. QuadMap: variable resolution maps to better represent spatial uncertainty. Comput. Geosci. 181, 105480. http://dx.doi.org/10.1016/j.cageo.2023.105480.

Pargent, F., Pfisterer, F., Thomas, J., Bischl, B., 2022. Regularized target encoding outperforms traditional methods in supervised machine learning with high cardinality features. Comput. Statist. 37 (5), 2671–2692. http://dx.doi.org/10.1007/s00180-022-01207-6.

Pebesma, E.J., 2004. Multivariable geostatistics in S: The gstat package. Comput. Geosci. 30, 683–691.

Pedregosa, F., Varoquaux, G., Gramfort, A., Michel, V., Thirion, B., Grisel, O., Blondel, M., Prettenhofer, P., Weiss, R., Dubourg, V., Vanderplas, J., Passos, A., Cournapeau, D., Brucher, M., Perrot, M., Duchesnay, E., 2011. Scikit-learn: Machine Learning in Python. J. Mach. Learn. Res. 12, 2825–2830.

Poeplau, C., Don, A., 2015. Carbon sequestration in agricultural soils via cultivation of cover crops – a meta-analysis. Agric. Ecosyst. Environ. 200, 33–41. http://dx.doi.org/10.1016/j.agee.2014.10.024.

Rogge, D., Bauer, A., Zeidler, J., Mueller, A., Esch, T., Heiden, U., 2018. Building an exposed soil composite processor (SCMaP) for mapping spatial and temporal characteristics of soils with landsat imagery (1984–2014). Remote Sens. Environ. 205, 1–17. http://dx.doi.org/10.1016/j.rse.2017.11.004.

Safanelli, J.L., Chabrillat, S., Ben-Dor, E., Demattê, J.A.M., 2020. Multispectral models from bare soil composites for mapping topsoil properties over Europe. Remote. Sens. 12 (9), 1369. http://dx.doi.org/10.3390/rs12091369.

Samarinas, N., Tsakiridis, N.L., Kokkas, S., Kalopesa, E., Zalidis, G.C., 2023. Soil data cube and artificial intelligence techniques for generating national-scale topsoil thematic maps: A Case Study in Lithuanian croplands. Remote. Sens. 15 (22), 5304. http://dx.doi.org/10.3390/rs15225304.

Shi, P., Castaldi, F., van Wesemael, B., Van Oost, K., 2020. Vis-NIR spectroscopic assessment of soil aggregate stability and aggregate size distribution in the Belgian Loam Belt. Geoderma 357, 113958. http://dx.doi.org/10.1016/j.geoderma.2019.113958.

Shi, P., Six, J., Sila, A., Vanlauwe, B., Van Oost, K., 2022. Towards spatially continuous mapping of soil organic carbon in croplands using multitemporal sentinel-2 remote sensing. ISPRS J. Photogramm. Remote Sens. 193, 187–199. http://dx.doi.org/10.1016/j.isprsjprs.2022.09.013.

Skakun, S., Wevers, J., Brockmann, C., Doxani, G., Aleksandrov, M., Batič, M., Frantz, D., Gascon, F., Gómez-Chova, L., Hagolle, O., López-Puigdollers, D., Louis, J., Lubej, M., Mateo-García, G., Osman, J., Peressutti, D., Pflug, B., Puc, J., Richter, R., Roger, J.-C., Scaramuzza, P., Vermote, E., Vesel, N., Zupanc, A., Žust, L., 2022. Cloud mask intercomparison exercise (CMIX): An evaluation of cloud masking algorithms for landsat 8 and sentinel-2. Remote Sens. Environ. 274, 112990. http://dx.doi.org/10.1016/j.rse.2022.112990.

Stenberg, B., Viscarra Rossel, R.A., Mouazen, A.M., Wetterlind, J., 2010. Chapter five - visible and near infrared spectroscopy in soil science. In: Sparks, D.L. (Ed.), Advances in Agronomy. vol. 107, Academic Press, pp. 163–215. http://dx.doi.org/10.1016/S0065-2113(10)07005-7.

Stevens, A., Nocita, M., Tóth, G., Montanarella, L., van Wesemael, B., 2013. Prediction of soil organic carbon at the European scale by visible and near InfraRed reflectance spectroscopy. PLOS ONE 8 (6), e66409. http://dx.doi.org/10.1371/journal.pone.0066409.

Stevens, A., van Wesemael, B., Bartholomeus, H., Rosillon, D., Tychon, B., Ben-Dor, E., 2008. Laboratory, field and airborne spectroscopy for monitoring organic carbon content in agricultural soils. Geoderma 144 (1), 395–404. http://dx.doi.org/10.1016/j.geoderma.2007.12.009.

Tian, X., de Bruin, S., Simoes, R., Isik, M.S., Minarik, R., Ho, Y.-F., Şahin, M., Herold, M., Consoli, D., Hengl, T., 2024. Spatiotemporal prediction of soil organic carbon density for europe (2000–2022) in 3D+T based on landsat-based spectral indices time-series. http://dx.doi.org/10.21203/rs.3.rs-5128244/v1.

Tziolas, N., Tsakiridis, N., Heiden, U., Van Wesemael, B., 2024. Soil organic carbon mapping utilizing convolutional neural networks and earth observation data, a case study in Bavaria state Germany. Geoderma 444, 116867. http://dx.doi.org/10.1016/j.geoderma.2024.116867.

Urbina-Salazar, D., Vaudour, E., Baghdadi, N., Ceschia, E., Richer-de-Forges, A.C., Lehmann, S., Arrouays, D., 2021. Using sentinel-2 images for soil organic carbon content mapping in croplands of southwestern France. the usefulness of sentinel-1/2 derived moisture maps and mismatches between sentinel images and sampling dates. Remote. Sens. 13 (24), 5115. http://dx.doi.org/10.3390/rs13245115.

Urbina-Salazar, D., Vaudour, E., Richer-de-Forges, A.C., Chen, S., Martelet, G., Baghdadi, N., Arrouays, D., 2023. Sentinel-2 and sentinel-1 bare soil temporal mosaics of 6-year periods for soil organic carbon content mapping in central France. Remote. Sens. 15 (9), 2410. http://dx.doi.org/10.3390/rs15092410.

van Wesemael, B., Abdelbaki, A., Ben-Dor, E., Chabrillat, S., d'Angelo, P., Demattê, J.A.M., Genova, G., Gholizadeh, A., Heiden, U., Karlshoefer, P., Milewski, R., Poggio, L., Sabetizade, M., Sanz, A., Schwind, P., Tsakiridis, N., Tziolas, N., Yagüe, J., Žížala, D., 2024. A European soil organic carbon monitoring system leveraging sentinel 2 imagery and the LUCAS soil data base. Geoderma 452, 117113. http://dx.doi.org/10.1016/j.geoderma.2024.117113.

Vanongeval, F., Van Orshoven, J., Gobin, A., 2024. Contribution of the sentinel-2 spring seedbed spectra to the digital mapping of soil organic carbon concentration. Geoderma 449, 116984. http://dx.doi.org/10.1016/j.geoderma.2024.116984.

Vaudour, E., Gholizadeh, A., Castaldi, F., Saberioon, M., Borůvka, L., Urbina-Salazar, D., Fouad, Y., Arrouays, D., Richer-de-Forges, A.C., Biney, J., Wetterlind, J., Van Wesemael, B., 2022. Satellite imagery to map topsoil organic carbon content over cultivated areas: An Overview. Remote. Sens. 14 (12), 2917. http://dx.doi.org/10.3390/rs14122917.

Vaudour, E., Gomez, C., Loiseau, T., Baghdadi, N., Loubet, B., Arrouays, D., Ali, L., Lagacherie, P., 2019. The impact of acquisition date on the prediction performance of topsoil organic carbon from sentinel-2 for croplands. Remote. Sens. 11 (18), 2143. http://dx.doi.org/10.3390/rs11182143.

Vaysse, K., Lagacherie, P., 2017. Using quantile regression forest to estimate uncertainty of digital soil mapping products. Geoderma 291, 55–64. http://dx.doi.org/10.1016/j.geoderma.2016.12.017.

Viscarra Rossel, R.A., Behrens, T., 2010. Using data mining to model and interpret soil diffuse reflectance spectra. Geoderma 158 (1), 46–54. http://dx.doi.org/10.1016/j.geoderma.2009.12.025.

Viscarra Rossel, R.A., Chappell, A., De Caritat, P., McKenzie, N.J., 2011. On the soil information content of visible–near infrared reflectance spectra. Eur. J. Soil Sci. 62 (3), 442–453. http://dx.doi.org/10.1111/j.1365-2389.2011.01372.x.

Viscarra Rossel, R.A., Shen, Z., Ramirez Lopez, L., Behrens, T., Shi, Z., Wetterlind, J., Sudduth, K.A., Stenberg, B., Guerrero, C., Gholizadeh, A., Ben-Dor, E., St Luce, M., Orellano, C., 2024. An imperative for soil spectroscopic modelling is to think global but fit local with transfer learning. Earth-Sci. Rev. 254, 104797. http://dx.doi.org/10.1016/j.earscirev.2024.104797.

Viscarra Rossel, R.A., Webster, R., Bui, E.N., Baldock, J.A., 2014. Baseline map of organic carbon in Australian soil to support national carbon accounting and monitoring under climate change. Global Change Biol. 20 (9), 2953–2970. http://dx.doi.org/10.1111/gcb.12569.

Wadoux, A.M.J.C., Courteille, L., Arrouays, D., De Carvalho Gomes, L., Cortet, J., Creamer, R.E., Eberhardt, E., Greve, M.H., Grüneberg, E., Harhoff, R., Heuvelink, G.B.M., Krahl, I., Lagacherie, P., Miko, L., Mulder, V.L., Pásztor, L., Pieper, S., Richer-de-Forges, A.C., Sánchez-Rodríguez, A.R., Rossiter, D., Steinhoff-Knopp, B., Stöckhardt, S., Szatmári, G., Takács, K., Tsiafouli, M., Vanwalleghem, T., Wellbrock, N., Wetterlind, J., 2024. On soil districts. Geoderma 452, 117065. http://dx.doi.org/10.1016/j.geoderma.2024.117065.

Wadoux, A.M.J.-C., Heuvelink, G.B.M., 2023. Uncertainty of spatial averages and totals of natural resource maps. Methods Ecol. Evol. 14 (5), 1320–1332. http://dx.doi.org/10.1111/2041-210X.14106.

Wadoux, A.M.J.-C., Molnar, C., 2022. Beyond prediction: Methods for interpreting complex models of soil variation. Geoderma 422, 115953. http://dx.doi.org/10.1016/j.geoderma.2022.115953.

Wadoux, A.M.J.-C., Saby, N.P.A., Martin, M.P., 2023. Shapley values reveal the drivers of soil organic carbon stock prediction. SOIL 9 (1), 21–38. http://dx.doi.org/10.5194/soil-9-21-2023.

Wadoux, A.M.J.-C., Samuel-Rosa, A., Poggio, L., Mulder, V.L., 2020. A note on knowledge discovery and machine learning in digital soil mapping. Eur. J. Soil Sci. 71 (2), 133–136. http://dx.doi.org/10.1111/ejss.12909.

Walkley, A., Black, I.A., 1934. An examination of the Degtjareff Method for determining soil organic matter, and a proposed modification of the chromic acid titration method. Soil Sci. 37 (1), 29–38. http://dx.doi.org/10.1097/00010694-193401000-00003.

Wright, M.N., Wager, S., Probst, P., 2024. Ranger: A Fast Implementation of random forests.

Zepp, S., Heiden, U., Bachmann, M., Wiesmeier, M., Steininger, M., van Wesemael, B., 2021. Estimation of soil organic carbon contents in croplands of Bavaria from SCMaP Soil Reflectance Composites. Remote. Sens. 13 (16), 3141. http://dx.doi.org/10.3390/rs13163141.

Zhou, Y., Chartin, C., Van Oost, K., van Wesemael, B., 2022. High-resolution soil organic carbon mapping at the field scale in Southern Belgium (Wallonia). Geoderma 422, 115929. http://dx.doi.org/10.1016/j.geoderma.2022.115929.

Žížala, D., Minařík, R., Zádorová, T., 2019. Soil organic carbon mapping using multispectral remote sensing data: Prediction Ability of data with different spatial and spectral resolutions. Remote. Sens. 11 (24), 2947. http://dx.doi.org/10.3390/rs11242947.